RSC Advances

This article can be cited before page numbers have been issued, to do this please use: M. Yang, Y. Qin, C. Chen, Y. Zhang, B. Li, T. Liu, H. Gong, B. Wang and H. Zhu, *RSC Adv.*, 2016, DOI: 10.1039/C5RA28141E.

ROYAL SOCIETY OF CHEMISTRY

www.rsc.org/advances

View Article Online
DOI: 10.1039/C5RA28141E

Synthesis, biological evaluation and molecular docking studies of novel 1-(4,5-dihydro-1*H*-pyrazol-1-yl)ethanone-containing 1-methylindol derivatives as potential tubulin assembling inhibitors

Meng-Ru Yang[†a], Ya-Juan Qin[†a], Chen Chen[a], Ya-Liang Zhang[a], Bo-Yan Li[a], Tian-Bao Liu[a], Hai-Bin Gong*[b], Bao-Zhong Wang*[a], Hai-Liang Zhu*[a]

Abstract: A series of novel compounds (**6a-6v**) containing 1-methylindol and 31-(4,5-dihydro-1*H*-pyrazol-1-yl)ethanone skeleton were designed, synthesized and biologically evaluated as potential tubulin polymerization inhibitors and anticancer agents. Among them, compound **6q** showed the most potent tubulin polymerization inhibitory activity (IC_{50} = 1.98 μM) and *in vitro* growth inhibitory activity against A549, MCF-7 and HepG2 cell lines, with IC_{50} values of 0.15 μM, 0.17 μM, and 0.25 μM respectively, being comparable to the positive control. Furthermore, compound **6q** was a potent inducer of apoptosis in A549 cells and it had typical cellular effects for microtubule interacting agents, causing arrest of the cell cycle in G2/M phase. Confocal microscopy assay and molecular docking results further demonstrated that **6q** could bind tightly to the colchicine-site of tubulin and act as an anti-tubulin agent. These studies, along with 3D-QSAR modeling provided an important basis for further optimization of compound **6q** as a potential anticancer agent.

Keywords: tubulin; inhibitors; 1-methylindol; pyrazoline; molecular docking

---

[a] *State Key Laboratory of Pharmaceutical Biotechnology, Nanjing University, Nanjing 210093, People's Republic of China*

[b] *Xuzhou Central Hospital, Xuzhou 221009, People's Republic of China*

* Corresponding author. Tel. & fax: +86-25-89682572. E-mail address: zhuhl@nju.edu.cn

† Both authors contributed equally to this work.

View Article Online
DOI: 10.1039/C5RA28141E

1. Introduction

Microtubules (MTs) are a broadly exploited target for the development of new effective anticancer agents. [1-3] MTs are highly dynamic polymers mainly composed of *α, β*-tubulin heterodimers which turn over continuously. Their polymerization-depolymerization dynamics play a crucial role in various fundamental cellular processes including mitotic spindle formation, organization of intracellular structure, and intracellular transport, as well as cell signaling and secretion. [4] Hence, interfering with MTs function can block cell division and cause cell damage, which is an established strategy to inhibit the proliferation of cancer cells. [2-3, 5]

There are many agents that bind to tubulin and interfere with microtubule assembly. Colchicine (compound **1**, **Figure 1**), one of the earliest tubulin-targeting drugs, can effectively interfere with microtubule polymerization and its binding site on tubulin has been characterized already. [6, 7] However, due to its highly adverse effects, the clinical development of colchicine for cancer therapy was not successful. [8] Another well-known potent anti-tubulin agent is CA-4 (compound **2**, **Figure 1**), which was isolated from the bark of the South African tree *Combretum caffrum*. It can potently bind to the colchicine binding site, leading to severe cytotoxicity against multiple human cancer cell lines. [9] But unfortunately, it easily undergoes *cis-trans* isomerization under natural light, causing a sharp reduction in the anti-tubulin activity, which limits its further applications. [10] Despite a long history of characterization, colchicine binding site inhibitors have not yet reached the commercial phase as anticancer drugs to date. Thus, further studies are required.

In the last two decades, an ever increasing number of synthetic indoles have been reported, which are able to inhibit tubulin polymerization, such as compound **3** (ATIs), [11] **4** (BPROL075) [12] and **5** [13] (**Figure 1).** It could be found that the indole structure is a crucial structural motif for tubulin inhibition. The indole nucleus also has been reported to be one of the core nucleuses for potent inhibitors of tubulin polymerization. [14, 15] Furthermore, the addition of methyl to the N atom of indole would be better for the inhibition of tubulin polymerization and cytotoxicity. [16, 17]

View Article Online
DOI: 10.1039/C5RA28141E

Also, pyrazolines have gained prominence due to its broad spectrum of biological activities including anticancer, antimicrobial and anti-inflammatory, [18, 19] as well as producing useful intermediates in several organic preparations. It was also reported some pyrazoline derivatives can inhibit tubulin polymerization by binding to the colchicine-site, such as compound **6**. [20] Besides, the presence of acetyl on the N atom of the five-membered ring enhances the inhibition of cell proliferation and the binding of the colchicine-site. For example, compound **7** (A-204197) [21] and compound **8** [22] (**Figure 1**) showed potent anti-proliferative activities against multiple cancer cell lines and tightly bound to the colchicine-site of tubulin.

Therefore, due to these previous researches and molecule modeling studies, we attempt to integrate 1-methylindol with 1-(4,5-dihydro-1*H*-pyrazol-1-yl)ethanone to screen novel compounds (**6a-6v**) as potential anti-tubulin agents (**Figure 1**). These coupling structures might possess enhanced anticancer activities. A series of novel 1-methylindol derivatives targeting tubulin were recently reported as potent anticancer agents in our group. [23] To extend our research and gain further insight in the ensuing structure–activity relationships (SARs), here we search more novel agents. Our strategy for further development of active anti-tubulin agents was to perform modifications on the two aromatic rings (A, B ring). Once the new combined scaffold was identified as the minimum structural requirement for activity in this new series of compounds, then some substituents were introduced onto the aromatic rings, and the modifications have been performed to screen a series of active anticancer agents.

So far, few reports have been dedicated to design and synthesize any anticancer compound containing 1-methylindol and 1-(4,5-dihydro-1*H*-pyrazol-1-yl)ethanone. Herein, we discussed the synthetic method and structure-activity relationship (SAR) of this series of compounds, evaluated their anticancer and anti-tubulin activities, and learned the influence on cell cycle and cell apoptosis. In addition, confocal microscopy assay provided a more directly view of the effect on microtubule system. Docking simulations are performed using the X-ray crystallographic structure of the tubulin in complex with an inhibitor to explore the binding modes of these

View Article Online
DOI: 10.1039/C5RA28141E

compounds at the active site.

2. Results and discussion

2.1. Chemistry

The synthetic route of compounds **6a-6v** (**Table 1**) was outlined in **Scheme 1**. First of all, the substituted 1*H*-indole (**1a-1c**) dissolved in DMF was added to a mixture of $POCl_3$ and DMF at 0 °C to generate compounds **2a-2c** after two-hour stirring. Then the substituted indole-3-carbaldehyde (**2a-2c**) was dissolved in THF and reacted with NaH and CH_3I to introduce the methyl group to the N atom of indole and obtain compounds **3a-3c.** Subsequently, the obtained compounds (**3a-3c**) and the corresponding acetophenone were dissolved in ethanol in the presence of KOH to give products **4a-4v.** After that, the obtained chalcone (**4a-4v**) was stirred with hydrazine hydrate in ethanol and refluxed for 2h, and then crude compounds **5a-5v** were gained. Finally, to a stirred solution of acetic acid, EDC·HCl and HOBt in acetonitrile or dichloromethane, obtained compounds (**5a-5v**) were added with the protection of N_2 to get the target compounds **6a-6v**. All synthesized compounds **6a-6v** are reported for the first time and determined by ^{1}H NMR, melting test, ESI-MS and elemental analysis, which were consistent with the assigned structures.

2.2. Crystal structure of compound 6o

The crystal structure of compound **6o** was determined by X-ray diffraction analysis. The crystal data presented in **Table 2** and **Figure 2** gave perspective views of compound **6o** with the atomic labeling system.

2.3. Biological activity

2.3.1. *In vitro* anti-proliferative activity

We prepared three different human cancer cell lines, including A549 (human nonsmall cell lung carcinoma), MCF-7 (human breast adenocarcinoma) and HepG2 (human liver hepatocellular carcinoma), and one normal cell line (293T) to evaluate

View Article Online
DOI: 10.1039/C5RA28141E

the anti-proliferative activities of all the synthesized compounds (**6a-6v**). The results were summarized in **Table 3.** Among all the 22 tested compounds, **6b**, **6i**, **6q**, **6t**, **6u** and **6v** possessed the highest overall potency with IC_{50} values ranging from 0.15 to 0.34 μM against all the three typical cancer cell lines. Compound **6q** was found to be the most active among all compounds with the level of IC_{50} values of 0.15 μM, 0.17 μM, and 0.25 μM against A549, MCF-7 and HepG2 cell lines respectively, superior to the positive compound colchicine. Besides, the results of 293T cell line indicated that these compounds possessed high safety.

Based on the data of **Table 3**, we found that the substituent group on the A-ring was of great importance to the activity of the tested compounds. Obviously, the anti-proliferative activities of compounds with different substituents in the A-ring increased in the following order: Br > H > OCH_3, which could be observed from the comparisons: **6n** > **6a** > **6h**, **6q** > **6i** > **6b** and **6v** > **6f** > **6m**.

The inhibitory activity of compounds with -OCH_3 on different positions of the B-ring increased in the following order: 4-OCH_3 (**6q**)> 3,4,5-$(OCH_3)_3$ (**6s**)> 3,4-$(OCH_3)_2$ (**6r**)> 2-OCH_3 (**6o**)> 3-OCH_3 (**6p**). Thus, we could draw a conclusion that compounds with *p*-substituted group showed the most potent activity, following by those of *o*-substituted, while *m*-substituted compounds had the lowest activity. Among all *p*-substituted (B-ring) compounds, **6n**, **6q**, **6t**, **6u** and **6v** (IC_{50} = 1.08 μM, 0.15μM, 0.21μM, 0.24μM, 0.18 μM) exhibited significant anti-proliferative activities in the order of -OCH_3> -Br > -F > -Cl > -H in A549 cell line, while **6a, 6b, 6e** and **6f, 6h, 6i, 6k, 6l** and **6m** showed the similar order.

2.3.2. Inhibition of tubulin polymerization

To investigate whether the anti-proliferative activities of compounds **6a-6v** were resulted from their interaction with tubulin, we evaluated the ability of these agents to inhibit tubulin polymerization *in vitro* (**Table 3**). These agents inhibited tubulin assembling with IC_{50} values ranging from 1.98 to 34.96 μM. Among them, compound **6q** showed the most potent activity of anti-tubulin (IC_{50} = 1.98 μM), better than the

View Article Online
DOI: 10.1039/C5RA28141E

positive control colchicine (2.35 μM). We also found that the IC_{50} values of tubulin polymerization of these compounds displayed a similar tendency with their relevant IC_{50} values of the anti-proliferative assay. **Figure 3** presented the relationship between the anti-proliferative activity against A549 cell line and the tubulin polymerization inhibitory activity of the top 10 compounds (**6b, 6f, 6i, 6o, 6q, 6r, 6s, 6t, 6u** and **6v**), which indicated that there was a moderate correlation between them with an R^2 value of 0.90. Therefore, we could conclude that most of the synthesized compounds could inhibit the tubulin assembly and the anti-proliferative effect was produced partly by their interaction with tubulin.

2.3.3. Compound 6q induced cell cycle arrest and cell apoptosis

To explore whether compound **6q** could arrest the process of mitosis, A549 cells were treated with **6q** of increasing concentrations (0.02 μM, 0.05 μM, 0.1 μM, 0.15 μM, 0.2 μM) for 24 h and then incubated with propidium iodide (PI) to analyze their genomic DNA content in flow cytometry assays (**Figure 4**). We found that, compound **6q** induced a gradual accumulation of cells in G2/M phase of the cell cycle in a dose-dependent manner with a rise in G2/M cells occurring at a concentration as low as 0.02 μM. When the concentration increased to 0.20 μM, up to 90% of the cells were arrested in the G2/M phase. In contrast, there was a continuing decrease in the proportion of cells in other phase (G1 and S) of the cell cycle.

To explore the correlation between cell cycle arrest and cell death induced by compound **6q**, a biparametric cytofluorimetric analysis using PI and annexin-V (stain DNA and phosphatidylserine residues, respectively) was performed. Dual staining of annexin-V and PI permits discrimination between early apoptotic cells (annexin-V^+/PI^-), late apoptotic cells (annexin-V^+/PI^+), live cells (annexin-V^-/PI^-) and necrotic cells (annexin-V^-/PI^+). A549 cells were treated with 0, 0.05, 0.1 and 0.15 μM of **6q** for 24 h. As shown in **Figure 5**, the percentage of both early and late apoptotic cells increased as the concentration of **6q** became higher, rising from 2.34% and 1.76% at 0 μM initially to 9.0% and 16.2% at 0.15 μM eventually. Thus, we could draw a

View Article Online
DOI: 10.1039/C5RA28141E

conclusion that compound **6q** could induce cell apoptosis in a dose-dependent manner.

2.3.4. Compound 6q inhibited tubulin polymerization and disrupted the microtubule system

Our results suggested that **6q** can target microtubules in A549 cells. To test this directly, we treated cells with 0.2 μM of **6q** for 24 h and analyzed microtubules by immunocytochemistry staining. As shown in **Figure 6**, the microtubule network of control cells displayed normal arrangement and organization, which was slim and fibrous. After treatment with 0.2 μM of **6q**, microtubules became short and wrapped around the nucleus. We also noted a significant reduction in the density of cellular microtubules and the radial organization of microtubules was perturbed, which could also be found in colchicine (0.5 μM)-treated cells which were used as positive control in this assay. In contrast, 0.5 μM of paclitaxel dramatically enhanced microtubule polymerization, with an increase in the density of cellular microtubules and formation of long thick microtubule bundles. These results further confirmed that the observed effects were due to interaction with tubulin, resulting in a prolonged mitotic arrest that ultimately leads to cell death.

2.4. Computational

2.4.1. Molecular docking

To gain a better understanding on the binding mode of the synthesized compounds, we proceeded to examine the interaction of compounds **6a-6v** with tubulin crystal structure (PDB code: 1SA0) using the DS 3.5 (Discovery Studio 3.5, Accelrys, Co. Ltd). The molecular docking was performed by inserting the compounds into the colchicine binding site of tubulin. Among them, compound **6q** showed the lowest interaction energy, at -54.27 kcal /mol. The binding models of compound **6q** and tubulin were depicted in **Figure 7**. The enzyme surface model (**Figure 7A**) revealed that the compound **6q** was well embedded in the active pocket

View Article Online
DOI: 10.1039/C5RA28141E

via hydrophobic interaction. The amino acid residues interacting with tubulin were labeled. The oxygen atom of acetyl contributes to the hydrogen bonding interaction with the hydrogen atom on the main chain of Ala B: 250 (angle N-H…O = 127.1°, distance = 2.47 Å). The 2D diagram of the interactions between the colchicine binding site and colchicine or compound **6q** were shown in **Figure 7C** and **D**, respectively. Significant similarities could be found in their tubulin-binding models. For example, residues Ala B: 250, Met B: 259, Cys B: 241, Leu B: 255, Leu B: 248 and Lys B: 352 were predicted to make contacts with colchicine or compound **6q**. Besides, **Figure 7B** presented a superimposition of these two compounds. This molecular docking results along with the biological assay data suggested that compound **6q** was a potential inhibitor of tubulin.

2.4.2. 3D-QSAR model

To obtain a systematic SAR profile on the synthesized compounds as antitumor agents and explore more potent and selective tubulin inhibitors, 3D-QSAR model was built by using the corresponding pIC_{50} values which were converted from the obtained IC_{50} (μM) values of tubulin inhibition (the way of this transformation was derived from an online calculator developed by an Indian Medicinal Chemistry Lab (http://www.sanjeevslab.org/tools-IC_{50}.html)) and performed by built-in QSAR software of DS 3.5. The training and test set were divided by the random diverse molecules method, where the training set accounted for 80% of all the molecules while the test was set to 20%, with 18 agents and 4 agents respectively. The observed and predicted values, corresponding residual values for the training set and test set molecules in 3D-QSAR model, were presented in **Table 4**. The graphical relationship of observed and predicted values was showed in **Figure 8**, in which the plot of the observed IC_{50} versus the predicted values showed that this model could be used in prediction of activity for 1-methylindol- and pyrazoline-containing derivatives. Also the molecules aligned with the iso-surfaces of the 3D-QSAR model coefficients on electrostatic potential grids (**Figure 9A**) and van der Waals grids (**Figure 9B**) were

View Article Online
DOI: 10.1039/C5RA28141E

listed. Electrostatic map indicated red contours around regions where high electron density (negative charge) was expected to increase activity, while blue contours represent areas where low electron density (partial positive charge) was expected to increase activity. This model is consistent with the docking results. For example, the red region near the B ring corresponds to the Lys B: 352 residue. Compounds **6b**, **6i** and **6q** could fit the red subregion, and this is part of the reason why these small molecules show potent tubulin inhibitory activity. Similarly, steric map indicated areas where steric bulk was predicted to increase (green) or decrease (yellow) activity. It was widely acceptable that a better inhibitor based on the 3D-QSAR model should have strong van der Waals attraction in the green areas and a polar group in the blue electrostatic potential areas (which were dominant close to the skeleton). This promising model would provide a guideline to design and optimize more effective tubulin inhibitors and pave the way for us in the further study.

3. Conclusions

In this study, a series of novel compounds (**6a-6v**) containing 1-methylindol and 1-(4,5-dihydro-1*H*-pyrazol-1-yl)ethanone skeleton were designed, synthesized and evaluated as potential inhibitors of tubulin polymerization. Most of them showed potent anti-proliferative activity, and compound **6q** displayed the most potent activity against tubulin assembling, A549, MCF-7 and HepG2 cell lines with IC_{50} values of 1.98 μM, 0.15 μM, 0.17 μM, and 0.25 μM respectively, which was comparable to the positive compound colchicine. Furthermore, the mechanism of action studies proved that compound **6q** could cause accumulation of cells in the G2/M phase of the cell cycle and potently induce apoptosis in A549 cells, as well as severe disruption of the microtubule system. Besides, molecular docking and 3D-QSAR were performed to learn the inhibitor-tubulin interactions. According to the analysis of the binding model of compound **6q** with tubulin, several interactions were observed with the protein residues in the colchicine binding site, which may contribute to its anti-tubulin polymerization and anti-proliferative activities. The research of these well designed

View Article Online
DOI: 10.1039/C5RA28141E

compounds might be greatly helpful for the development of tubulin polymerization inhibitors with stronger activities in the future.

4. Experiments

4.1. Chemistry general

All reagents and solvents were of analysis or synthesis grade. Melting points were determined on a XT4MP apparatus (Taike Corp, Beijing, China). ^{1}H NMR spectra were recorded on a Bruker DPX300 model Spectrometer using tetramethylsilane (TMS) as internal standard and DMSO or $CDCl_3$ as solvents (chemical shifts in ppm (d)). TLC was performed on the glass backed silica gel sheets (Silica Gel 60 GF254) and visualized in UV light (254 nm and 365 nm). ESI-MS spectra were recorded on a Mariner System 5304 Mass spectrometer. Elemental analyses were performed on a CHN-O-Rapid instrument and were within ± 0.4% of the theoretical values.

4.1.1. General procedure for the synthesis of 1*H*-indole-3-carbaldehyde (2a)

To a stirred and completely mixed solution of $POCl_3$ (20 mL) in DMF (40 mL), **1a** (35 mmol) in DMF (40 mL) was added at 0 °C. After a further 2 h reaction, the mixture was poured into 300 mL ice water and mixed completely. Then NaOH pellets were added and adjusted the pH to 9.0. The reaction mixture was filtered, and washed with ethyl acetate. Then the filtrate was extracted by ethyl acetate. The organic layer was dried over Na_2SO_4 and concentrated to give a brown solid, yield 98.1%. The crude **2a** was used in the next step without any further purification. Following this way, we got crude compounds **2a-2c** with yields of 95.3-98.1%.

4.1.2. General procedure for the synthesis of 1-methyl-1*H*-indole-3-carbaldehyde (3a)

To a stirred solution of **2a** (25 mmol) in THF (15 mL) at 0 °C was added NaH (62.5 mmol) in THF (15 mL) slowly and stirred for 15 min. Then CH_3I (33 mmol)

View Article Online
DOI: 10.1039/C5RA28141E

was added and the reaction mixture was moved to room temperature to react for further 24 h. The reaction was stopped after the consumption of the starting material monitored by TLC. Then the solution was removed and the mixture was extracted by ethyl acetate. The organic layer was washed with brine, dried over Na_2SO_4 and concentrated to give crude residue**, 3a**, yield 97.5%. Following this way, we got crude compounds **3a-3c** with yields of 93.4-97.5%.

4.1.3. General procedure for the synthesis of (*E*)-3-(1-methyl-1*H*-indol-3-yl)-1-phenylprop-2-en-1-one (4a)

To a stirred solution of **3a** (2 mmol) and acetophenone (2 mmol) in ethanol (20 mL), KOH (6 mmol, 336 mg) was added at room temperature. After the reaction was completed (24 h), the reaction mixture was filtered and washed with water and cool ethanol. The crude product was purified by recrystallization from ethanol and dichloromethane to give **4a**, a yellow crystal, yield 93.1%. Following this way, we got pure compounds **4a-4v** with yields of 38.5-95.7%.

4.1.4. General procedure for the synthesis of 1-methyl-3-(3-phenyl-4,5-dihydro-1*H*-pyrazol-5-yl)-1*H*-indole (5a)

A mixture of **4a** (1 mmol) and hydrazine hydrate (2 mmol) was dissolved in ethanol (5 mL) and refluxed for 2h. The reaction mixture was cooled and kept at -20 °C overnight. Then the solid obtained was filtered off and washed with petroleum ether and taken for the next step immediately. Following this way, we got crude compounds **5a-5v**.

4.1.5. General procedure for the synthesis of 1-(5-(1-methyl-1*H*-indol-3-yl)-3-phenyl-4,5-dihydro-1*H*-pyrazol-1-yl)ethanone (6a)

To a stirred solution of acetic acid (2 mmol), EDC·HCl (3 mmol) and HOBt (1.2 mmol) in acetonitrile or dichloromethane (5 mL), **5a** (1 mmol) was added at room

View Article Online
DOI: 10.1039/C5RA28141E

temperature with the protection of N_2. After 24 h, the reaction mixture was filtered and washed with cool ethanol and water. The crude product was purified by recrystallization from ethanol and dichloromethane to give **6a**, a white powder, yield 30.2%. Following this way, we got pure compounds **6a-6v**.

White powder. Yield: 30.2%. m. p. 171 ~ 172 °C. ^{1}H NMR (DMSO-d_6, 400 MHz) δ: 7.93 – 7.76 (m, 2H), 7.57 – 7.43 (m, 3H), 7.40 (d, J = 8.2 Hz, 1H), 7.33 (d, J = 7.9 Hz, 1H), 7.25 (s, 1H), 7.13 (t, J = 7.4 Hz, 1H), 6.97 (t, J = 7.3 Hz, 1H), 5.81 (dd, J = 11.8, 4.4 Hz, 1H), 3.84 (dd, J = 18.0, 11.9 Hz, 1H), 3.72 (s, 3H), 3.25 (dd, J = 18.0, 4.4 Hz, 1H), 2.26 (s, 3H). MS (ESI) *m/z*: 318.15 ($C_{20}H_{19}N_3O$, $[M+H]^+$). Anal. Calcd for $C_{20}H_{19}N_3O$: C, 75.69; H, 6.03; N, 13.24. Found: C, 75.81; H, 6.04; N, 13.22.

4.1.6.

1-(3-(4-methoxyphenyl)-5-(1-methyl-1*H*-indol-3-yl)-4,5-dihydro-1*H*-pyrazol-1-yl) ethan-1-one (6b)

Brown crystal. Yield: 34.5%. m. p. 156 ~ 158 °C. ^{1}H NMR (DMSO-d_6, 400 MHz) δ: 7.77 (d, J = 8.8 Hz, 2H), 7.39 (d, J = 8.2 Hz, 1H), 7.33 (d, J = 7.9 Hz, 1H), 7.23 (s, 1H), 7.13 (t, J = 7.4 Hz, 1H), 7.03 (d, J = 8.8 Hz, 2H), 6.96 (t, J = 7.4 Hz, 1H), 5.77 (dd, J = 11.8, 4.2 Hz, 1H), 3.87 – 3.75 (m, 4H), 3.72 (s, 3H), 3.22 (dd, J = 17.9, 4.3 Hz, 1H), 2.23 (s, 3H). MS (ESI) *m/z*: 348.16 ($C_{21}H_{21}N_3O_2$, $[M+H]^+$). Anal. Calcd for $C_{21}H_{21}N_3O_2$: C, 72.60; H, 6.09; N, 12.10. Found: C, 72.54; H, 6.09; N, 12.11.

4.1.7.

1-(3-(3,4-dimethoxyphenyl)-5-(1-methyl-1*H*-indol-3-yl)-4,5-dihydro-1*H*-pyrazol-1 -yl)ethan-1-one (6c)

Brown crystal. Yield: 14.3%. m. p. 169 ~ 171 °C. ^{1}H NMR (DMSO-d_6, 400 MHz) δ: 7.39 (d, J = 8.4 Hz, 2H), 7.36 – 7.29 (m, 2H), 7.23 (s, 1H), 7.13 (t, J = 7.6 Hz, 1H), 7.02 (d, J = 8.4 Hz, 1H), 6.97 (t, J = 7.5 Hz, 1H), 5.78 (dd, J = 11.7, 4.2 Hz, 1H), 3.88 – 3.75 (m, 7H), 3.72 (s, 3H), 3.25 (dd, J = 17.8, 4.3 Hz, 1H), 2.25 (s, 3H). MS (ESI) *m/z*: 378.17 ($C_{22}H_{23}N_3O_3$, $[M+H]^+$). Anal. Calcd for $C_{22}H_{23}N_3O_3$: C, 70.01; H, 6.14; N,

View Article Online
DOI: 10.1039/C5RA28141E

11.13. Found: C, 69.90; H, 6.15; N, 11.15.

4.1.8.

1-(5-(1-methyl-1*H*-indol-3-yl)-3-(3,4,5-trimethoxyphenyl)-4,5-dihydro-1*H*-pyrazol-1-yl)ethan-1-one (6d)

White powder. Yield: 43.1%. m. p. 224 ~ 226 °C. ^{1}H NMR (DMSO-d_6, 400 MHz) δ: 7.38 (t, J = 8.7 Hz, 2H), 7.22 (s, 1H), 7.14 (t, J = 7.6 Hz, 1H), 7.09 (s, 2H), 6.99 (t, J = 7.4 Hz, 1H), 5.81 (dd, J = 11.7, 4.2 Hz, 1H), 3.87 – 3.76 (m, 7H), 3.72 (d, J = 5.5 Hz, 6H), 3.32 (dd, J = 17.9, 4.4 Hz, 1H), 2.27 (s, 3H). MS (ESI) *m/z*: 408.18 ($C_{23}H_{25}N_3O_4$, $[M+H]^+$). Anal. Calcd for $C_{23}H_{25}N_3O_4$: C, 67.80; H, 6.18; N, 10.31. Found: C, 67.95; H, 6.17; N, 10.33.

4.1.9.

1-(3-(4-chlorophenyl)-5-(1-methyl-1*H*-indol-3-yl)-4,5-dihydro-1*H*-pyrazol-1-yl)ethan-1-one (6e)

White powder. Yield: 11.1%. m. p. 182 ~ 183 °C. ^{1}H NMR (DMSO-d_6, 400 MHz) δ: 7.84 (d, J = 8.6 Hz, 2H), 7.55 (d, J = 8.6 Hz, 2H), 7.40 (d, J = 8.2 Hz, 1H), 7.32 (d, J = 7.9 Hz, 1H), 7.25 (s, 1H), 7.13 (t, J = 7.6 Hz, 1H), 6.97 (t, J = 7.5 Hz, 1H), 5.81 (dd, J = 11.8, 4.4 Hz, 1H), 3.83 (dd, J = 18.0, 11.9 Hz, 1H), 3.72 (s, 3H), 3.25 (dd, J = 18.0, 4.5 Hz, 1H), 2.25 (s, 3H). MS (ESI) *m/z*: 352.11 ($C_{20}H_{18}ClN_3O$, $[M+H]^+$). Anal. Calcd for $C_{20}H_{18}ClN_3O$: C, 68.28; H, 5.16; N, 11.94. Found: C, 68.21; H, 5.15; N, 11.96.

4.1.10.

1-(3-(4-bromophenyl)-5-(1-methyl-1*H*-indol-3-yl)-4,5-dihydro-1*H*-pyrazol-1-yl)ethan-1-one (6f)

White powder. Yield: 17.7%. m. p. 183 ~ 185 °C. ^{1}H NMR (DMSO-d_6, 400 MHz) δ: 7.77 (d, J = 8.6 Hz, 2H), 7.68 (d, J = 8.6 Hz, 2H), 7.39 (d, J = 8.2 Hz, 1H), 7.32 (d, J = 7.9 Hz, 1H), 7.25 (s, 1H), 7.13 (t, J = 7.4 Hz, 1H), 6.97 (t, J = 7.4 Hz, 1H), 5.81

View Article Online
DOI: 10.1039/C5RA28141E

(dd, *J* = 11.9, 4.4 Hz, 1H), 3.83 (dd, *J* = 18.0, 11.9 Hz, 1H), 3.72 (s, 3H), 3.25 (dd, *J* = 18.0, 4.5 Hz, 1H), 2.25 (s, 3H). MS (ESI) *m/z*: 396.06($C_{20}H_{18}BrN_3O$, $[M+H]^+$). Anal. Calcd for $C_{20}H_{18}BrN_3O$: C, 60.62; H, 4.58; N, 10.60. Found: C, 60.67; H, 4.59; N, 10.58.

4.1.11.

1-(5-(1-methyl-1*H*-indol-3-yl)-3-(4-(trifluoromethyl)phenyl)-4,5-dihydro-1*H*-pyrazol-1-yl)ethan-1-one (6g)

White crystal. Yield: 61.6%. m. p. 218 ~ 220 °C. ^{1}H NMR (DMSO-d_6, 400 MHz) δ: 8.04 (d, *J* = 8.1 Hz, 2H), 7.84 (d, *J* = 8.3 Hz, 2H), 7.40 (d, *J* = 8.2 Hz, 1H), 7.33 (d, *J* = 7.9 Hz, 1H), 7.28 (s, 1H), 7.14 (t, *J* = 7.5 Hz, 1H), 6.98 (t, *J* = 7.4 Hz, 1H), 5.85 (dd, *J* = 11.9, 4.5 Hz, 1H), 3.89 (dd, *J* = 18.1, 12.0 Hz, 1H), 3.73 (s, 3H), 3.33 – 3.22 (m, 1H), 2.28 (s, 3H). MS (ESI) *m/z*: 386.14 ($C_{21}H_{18}F_3N_3O$, $[M+H]^+$). Anal. Calcd for $C_{21}H_{18}F_3N_3O$: C, 65.45; H, 4.71; N, 10.90. Found: C, 65.31; H, 4.70; N, 10.87.

4.1.12.

1-(5-(5-methoxy-1-methyl-1*H*-indol-3-yl)-3-phenyl-4,5-dihydro-1*H*-pyrazol-1-yl)ethan-1-one (6h)

White crystal. Yield: 45.0%. m. p. 175 ~ 176 °C. ^{1}H NMR (DMSO-d_6, 400 MHz) δ: 7.93 – 7.79 (m, 2H), 7.56 – 7.42 (m, 3H), 7.29 (d, *J* = 8.8 Hz, 1H), 7.20 (s, 1H), 6.80 (s, 1H), 6.77 (d, *J* = 8.8 Hz, 1H), 5.78 (dd, *J* = 11.7, 3.8 Hz, 1H), 3.82 (dd, *J* = 17.9, 11.7 Hz, 1H), 3.68 (s, 3H), 3.54 (s, 3H), 3.25 (dd, *J* = 17.9, 3.9 Hz, 1H), 2.26 (s, 3H). MS (ESI) *m/z*: 348.16 ($C_{21}H_{21}N_3O_2$, $[M+H]^+$). Anal. Calcd for $C_{21}H_{21}N_3O_2$: C, 72.60; H, 6.09; N, 12.10. Found: C, 72.71; H, 6.10; N, 12.12.

4.1.13.

1-(5-(5-methoxy-1-methyl-1*H*-indol-3-yl)-3-(4-methoxyphenyl)-4,5-dihydro-1*H*-pyrazol-1-yl)ethan-1-one (6i)

Light yellow powder. Yield: 46.7%. m. p. 158 ~ 160 °C. ^{1}H NMR (DMSO-d_6,

View Article Online
DOI: 10.1039/C5RA28141E

400 MHz) δ: 7.78 (d, J = 8.8 Hz, 2H), 7.28 (d, J = 8.8 Hz, 1H), 7.18 (s, 1H), 7.03 (d, J = 8.9 Hz, 2H), 6.81 (s, 1H), 6.77 (d, J = 8.8 Hz, 1H), 5.75 (dd, J = 11.6, 3.8 Hz, 1H), 3.84 – 3.69 (m, 4H), 3.68 (s, 3H), 3.56 (s, 3H), 3.21 (dd, J = 17.8, 3.9 Hz, 1H), 2.23 (s, 3H). MS (ESI) *m/z*: 378.17 ($C_{22}H_{23}N_3O_3$, $[M+H]^+$). Anal. Calcd for $C_{22}H_{23}N_3O_3$: C, 70.01; H, 6.14; N, 11.13. Found: C, 69.91; H, 6.16; N, 11.13.

4.1.14.

1-(3-(3,4-dimethoxyphenyl)-5-(5-methoxy-1-methyl-1*H*-indol-3-yl)-4,5-dihydro-1*H*-pyrazol-1-yl)ethan-1-one (6j)

Grey solid. Yield: 10.2%. m. p. 186 ~ 187 °C. ^{1}H NMR (DMSO-d_6, 400 MHz) δ: 7.42 (s, 1H), 7.34 (d, J = 8.3 Hz, 1H), 7.29 (d, J = 8.8 Hz, 1H), 7.17 (s, 1H), 7.03 (d, J = 8.4 Hz, 1H), 6.83 (s, 1H), 6.78 (d, J = 8.8 Hz, 1H), 5.76 (dd, J = 11.5, 3.4 Hz, 1H), 3.86 – 3.72 (m, 7H), 3.68 (s, 3H), 3.58 (s, 3H), 3.24 (dd, J = 17.7, 3.6 Hz, 1H), 2.25 (s, 3H). MS (ESI) *m/z*: 408.18 ($C_{23}H_{25}N_3O_4$, $[M+H]^+$). Anal. Calcd for $C_{23}H_{25}N_3O_4$: C, 67.80; H, 6.18; N, 10.31. Found: C, 67.93; H, 6.17; N, 10.32.

4.1.15.

1-(3-(4-fluorophenyl)-5-(5-methoxy-1-methyl-1*H*-indol-3-yl)-4,5-dihydro-1*H*-pyrazol-1-yl)ethan-1-one (6k)

Gray powder. Yield: 29.8%. m. p. 178 ~ 180 °C. ^{1}H NMR (DMSO-d_6, 400 MHz) δ: 7.90 (dd, J = 8.7, 5.5 Hz, 2H), 7.31 (dd, J = 18.0, 8.9 Hz, 3H), 7.19 (s, 1H), 6.85 – 6.73 (m, 2H), 5.78 (dd, J = 11.7, 3.8 Hz, 1H), 3.82 (dd, J = 17.9, 11.8 Hz, 1H), 3.68 (s, 3H), 3.57 (s, 3H), 3.25 (dd, J = 17.9, 3.9 Hz, 1H), 2.25 (s, 3H). MS (ESI) *m/z*: 366.15 ($C_{21}H_{20}FN_3O_2$, $[M+H]^+$). Anal. Calcd for $C_{21}H_{20}FN_3O_2$: C, 69.03; H, 5.52; N, 11.50. Found: C, 69.31; H, 5.51; N, 11.48.

4.1.16.

1-(3-(4-chlorophenyl)-5-(5-methoxy-1-methyl-1*H*-indol-3-yl)-4,5-dihydro-1*H*-pyrazol-1-yl)ethan-1-one (6l)

View Article Online
DOI: 10.1039/C5RA28141E

White crystal. Yield: 36.7%. m. p. 169 ~ 170 °C. ^{1}H NMR (DMSO-d_6, 400 MHz) δ: 7.86 (d, J = 8.6 Hz, 2H), 7.55 (d, J = 8.6 Hz, 2H), 7.29 (d, J = 8.6 Hz, 1H), 7.20 (s, 1H), 6.78 (d, J = 8.7 Hz, 2H), 5.79 (dd, J = 11.7, 3.9 Hz, 1H), 3.81 (dd, J = 18.0, 11.8 Hz, 1H), 3.68 (s, 3H), 3.57 (s, 3H), 3.24 (dd, J = 17.9, 4.0 Hz, 1H), 2.25 (s, 3H). MS (ESI) *m/z*: 382.12 ($C_{21}H_{20}ClN_3O_2$, $[M+H]^+$). Anal. Calcd for $C_{21}H_{20}ClN_3O_2$: C, 66.05; H, 5.28; N, 11.00. Found: C, 65.98; H, 5.27; N, 10.98.

4.1.17.

1-(3-(4-bromophenyl)-5-(5-methoxy-1-methyl-1*H*-indol-3-yl)-4,5-dihydro-1*H*-pyrazol-1-yl)ethan-1-one (6m)

White crystal. Yield: 38.6%. m. p. 172 ~ 173 °C. ^{1}H NMR (DMSO-d_6, 400 MHz) δ: 7.78 (d, J = 8.5 Hz, 2H), 7.68 (d, J = 8.4 Hz, 2H), 7.29 (d, J = 8.5 Hz, 1H), 7.19 (s, 1H), 6.78 (d, J = 8.6 Hz, 2H), 5.79 (dd, J = 11.7, 3.9 Hz, 1H), 3.81 (dd, J = 18.0, 11.9 Hz, 1H), 3.68 (s, 3H), 3.58 (s, 3H), 3.24 (dd, J = 18.0, 4.0 Hz, 1H), 2.25 (s, 3H). MS (ESI) *m/z*: 426.07 ($C_{21}H_{20}BrN_3O_2$, $[M+H]^+$). Anal. Calcd for $C_{21}H_{20}BrN_3O_2$: C, 59.17; H, 4.73; N, 9.86. Found: C, 59.33; H, 4.71; N, 9.85.

4.1.18.

1-(5-(5-bromo-1-methyl-1*H*-indol-3-yl)-3-phenyl-4,5-dihydro-1*H*-pyrazol-1-yl)ethan-1-one (6n)

White powder. Yield: 59.0%. m. p. 173 ~ 174 °C. ^{1}H NMR (DMSO-d_6, 400 MHz) δ: 7.94 – 7.74 (m, 2H), 7.61 (s, 1H), 7.57 – 7.41 (m, 3H), 7.39 (d, J = 8.7 Hz, 1H), 7.29 (s, 1H), 7.25 (d, J = 8.7 Hz, 1H), 5.81 (dd, J = 11.7, 4.2 Hz, 1H), 3.84 (dd, J = 18.0, 11.8 Hz, 1H), 3.72 (s, 3H), 3.25 (dd, J = 18.0, 4.3 Hz, 1H), 2.27 (s, 3H). MS (ESI) *m/z*: 396.06 ($C_{20}H_{18}BrN_3O$, $[M+H]^+$). Anal. Calcd for $C_{20}H_{18}BrN_3O$: C, 60.62; H, 4.58; N, 10.60. Found: C, 60.79; H, 4.57; N, 10.63.

4.1.19.

1-(5-(5-bromo-1-methyl-1*H*-indol-3-yl)-3-(2-methoxyphenyl)-4,5-dihydro-1*H*-pyr

View Article Online
DOI: 10.1039/C5RA28141E

azol-1-yl)ethan-1-one (6o)

Light yellow crystal. Yield: 58.5%. m. p. 180 ~ 181 °C. ^{1}H NMR (DMSO-d_6, 400 MHz) δ: 7.85 (d, J = 6.1 Hz, 1H), 7.63 (s, 1H), 7.46 (t, J = 7.0 Hz, 1H), 7.39 (d, J = 8.7 Hz, 1H), 7.30 (s, 1H), 7.25 (d, J = 6.9 Hz, 1H), 7.14 (d, J = 8.3 Hz, 1H), 7.06 (t, J = 7.9 Hz, 1H), 5.74 (dd, J = 11.8, 4.2 Hz, 1H), 3.88 (dd, J = 18.5, 11.8 Hz, 1H), 3.81 (s, 3H), 3.73 (s, 3H), 3.28 (dd, J = 18.5, 4.2 Hz, 1H), 2.23 (s, 3H). MS (ESI) *m/z*: 426.07 ($C_{21}H_{20}BrN_3O_2$, $[M+H]^+$). Anal. Calcd for $C_{21}H_{20}BrN_3O_2$: C, 59.17; H, 4.73; N, 9.86. Found: C, 59.31; H, 4.74; N, 9.84.

4.1.20.

1-(5-(5-bromo-1-methyl-1*H*-indol-3-yl)-3-(3-methoxyphenyl)-4,5-dihydro-1*H*-pyr azol-1-yl)ethan-1-one (6p)

White crystal. Yield: 59.9%. m. p. 184 ~ 185 °C. ^{1}H NMR (DMSO-d_6, 400 MHz) δ: 7.60 (s, 1H), 7.44 – 7.36 (m, 3H), 7.34 (s, 1H), 7.29 (s, 1H), 7.26 (d, J = 6.9 Hz, 1H), 7.11 – 7.02 (m, 1H), 5.80 (dd, J = 11.7, 4.3 Hz, 1H), 3.89 – 3.78 (m, 4H), 3.72 (s, 3H), 3.26 (dd, J = 18.0, 4.3 Hz, 1H), 2.27 (s, 3H). MS (ESI) *m/z*: 426.07 ($C_{21}H_{20}BrN_3O_2$, $[M+H]^+$). Anal. Calcd for $C_{21}H_{20}BrN_3O_2$: C, 59.17; H, 4.73; N, 9.86. Found: C, 59.24; H, 4.72; N, 9.87.

4.1.21.

1-(5-(5-bromo-1-methyl-1*H*-indol-3-yl)-3-(4-methoxyphenyl)-4,5-dihydro-1*H*-pyr azol-1-yl)ethan-1-one (6q)

White crystal. Yield: 75.8%. m. p. 208 ~ 209 °C. ^{1}H NMR (DMSO-d_6, 400 MHz) δ: 7.77 (d, J = 8.8 Hz, 2H), 7.59 (s, 1H), 7.39 (d, J = 8.7 Hz, 1H), 7.28 (s, 1H), 7.25 (d, J = 7.0 Hz, 1H), 7.03 (d, J = 8.8 Hz, 2H), 5.77 (dd, J = 11.6, 4.1 Hz, 1H), 3.91 – 3.75 (m, 4H), 3.72 (s, 3H), 3.21 (dd, J = 17.9, 4.2 Hz, 1H), 2.25 (s, 3H). MS (ESI) *m/z*: 426.07 ($C_{21}H_{20}BrN_3O_2$, $[M+H]^+$). Anal. Calcd for $C_{21}H_{20}BrN_3O_2$: C, 59.17; H, 4.73; N, 9.86. Found: C, 59.19; H, 4.72; N, 9.85.

View Article Online
DOI: 10.1039/C5RA28141E

4.1.22.

1-(5-(5-bromo-1-methyl-1*H*-indol-3-yl)-3-(3,4-dimethoxyphenyl)-4,5-dihydro-1*H*-pyrazol-1-yl)ethan-1-one (6r)

White powder. Yield: 64.8%. m. p. 229 ~ 231 °C. ^{1}H NMR (DMSO-d_6, 400 MHz) δ: 7.61 (s, 1H), 7.43 – 7.36 (m, 2H), 7.33 (d, J = 8.3 Hz, 1H), 7.26 (d, J = 9.1 Hz, 2H), 7.03 (d, J = 8.4 Hz, 1H), 5.78 (dd, J = 11.6, 4.0 Hz, 1H), 3.85 – 3.75 (m, 7H), 3.72 (s, 3H), 3.24 (dd, J = 17.9, 4.1 Hz, 1H), 2.27 (s, 3H). MS (ESI) *m/z*: 456.08 ($C_{22}H_{22}BrN_3O_3$, $[M+H]^+$). Anal. Calcd for $C_{22}H_{22}BrN_3O_3$: C, 57.90; H, 4.86; N, 9.21. Found: C, 57.98; H, 4.87; N, 9.22.

4.1.23.

1-(5-(5-bromo-1-methyl-1*H*-indol-3-yl)-3-(3,4,5-trimethoxyphenyl)-4,5-dihydro-1*H*-pyrazol-1-yl)ethan-1-one (6s)

Pink powder. Yield: 40.6%. m. p. 228 ~ 229 °C. ^{1}H NMR (DMSO-d_6, 400 MHz) δ: 7.65 (s, 1H), 7.39 (d, J = 8.7 Hz, 1H), 7.26 (t, J = 5.1 Hz, 2H), 7.09 (s, 2H), 5.82 (dd, J = 11.6, 4.1 Hz, 1H), 3.87 – 3.76 (m, 7H), 3.72 (s, 6H), 3.30 – 3.28 (m, 1H), 2.29 (s, 3H). MS (ESI) *m/z*: 486.10 ($C_{23}H_{24}BrN_3O_4$, $[M+H]^+$). Anal. Calcd for $C_{23}H_{24}BrN_3O_4$: C, 56.80; H, 4.97; N, 8.64. Found: C, 56.81; H, 4.97; N, 8.62.

4.1.24.

1-(5-(5-bromo-1-methyl-1*H*-indol-3-yl)-3-(4-fluorophenyl)-4,5-dihydro-1*H*-pyrazol-1-yl)ethan-1-one (6t)

White solid. Yield: 38.6%. m. p. 199 ~ 200 °C. ^{1}H NMR (DMSO-d_6, 400 MHz) δ: 7.89 (dd, J = 8.7, 5.5 Hz, 2H), 7.60 (s, 1H), 7.39 (d, J = 8.7 Hz, 1H), 7.33 (t, J = 8.9 Hz, 2H), 7.30 (s, 1H), 7.25 (d, J = 6.9 Hz, 1H), 5.81 (dd, J = 11.7, 4.2 Hz, 1H), 3.83 (dd, J = 18.0, 11.7 Hz, 1H), 3.72 (s, 3H), 3.26 (dd, J = 18.0, 4.3 Hz, 1H), 2.26 (s, 3H). MS (ESI) *m/z*: 414.05 ($C_{20}H_{17}BrFN_3O$, $[M+H]^+$). Anal. Calcd for $C_{20}H_{17}BrFN_3O$: C, 57.99; H, 4.14; N, 10.14. Found: C, 57.88; H, 4.14; N, 10.16.

View Article Online
DOI: 10.1039/C5RA28141E

4.1.25.

1-(5-(5-bromo-1-methyl-1*H*-indol-3-yl)-3-(4-chlorophenyl)-4,5-dihydro-1*H*-pyrazol-1-yl)ethan-1-one (6u)

White powder. Yield: 48.5%. m. p. 200 ~ 201 °C. ^{1}H NMR (DMSO-d_6, 400 MHz) δ: 7.84 (d, J = 8.5 Hz, 2H), 7.60 (s, 1H), 7.54 (d, J = 8.5 Hz, 2H), 7.38 (d, J = 8.7 Hz, 1H), 7.29 (s, 1H), 7.25 (d, J = 8.7 Hz, 1H), 5.81 (dd, J = 11.7, 4.1 Hz, 1H), 3.82 (dd, J = 18.0, 11.8 Hz, 1H), 3.71 (s, 3H), 3.25 (dd, J = 18.0, 4.3 Hz, 1H), 2.27 (s, 3H). MS (ESI) *m/z*: 430.02 ($C_{20}H_{17}BrClN_3O$, $[M+H]^+$). Anal. Calcd for $C_{20}H_{17}BrClN_3O$: C, 55.77; H, 3.98; N, 9.76. Found: C, 55.91; H, 3.97; N, 9.78.

4.1.26.

1-(5-(5-bromo-1-methyl-1*H*-indol-3-yl)-3-(4-bromophenyl)-4,5-dihydro-1*H*-pyrazol-1-yl)ethan-1-one (6v)

White powder. Yield: 37.0%. m. p. 206 ~ 207 °C. ^{1}H NMR (DMSO-d_6, 400 MHz) δ: 7.77 (d, J = 8.5 Hz, 2H), 7.68 (d, J = 8.6 Hz, 2H), 7.59 (s, 1H), 7.39 (d, J = 8.7 Hz, 1H), 7.30 (s, 1H), 7.25 (d, J = 7.0 Hz, 1H), 5.81 (dd, J = 11.7, 4.3 Hz, 1H), 3.82 (dd, J = 18.0, 11.8 Hz, 1H), 3.72 (s, 3H), 3.25 (dd, J = 18.0, 4.4 Hz, 1H), 2.27 (s, 3H). MS (ESI) *m/z*: 473.97 ($C_{20}H_{17}Br_2N_3O$, $[M+H]^+$). Anal. Calcd for $C_{20}H_{17}Br_2N_3O$: C, 50.55; H, 3.61; N, 8.84. Found: C, 50.42; H, 3.61; N, 8.86.

4.2. Crystal structure determination

Crystal structure determination of compound **6o** was carried out on a Nonius CAD4 diffractometer equipped with graphite-mono chromated Mo*Ka* (k = 0.71073 Å) radiation. The structure was solved by direct methods and refined on F^2 by full-matrix least-squares methods using SHELX-97. [24] All non-hydrogen atoms of compound **6o** were refined anisotropically. All hydrogen atoms were placed in geometrically idealized positions and constrained to ride on their respective parent atoms.

View Article Online
DOI: 10.1039/C5RA28141E

4.3. Biological assays

4.3.1. Anti-proliferation activity

Human nonsmall cell lung carcinoma (A549), human breast adenocarcinoma (MCF-7), human liver hepatocellular carcinoma (HepG2) and human renal epithelial cells (293T) were cultured in DMEM supplemented with 10% fetal bovine serum, 115 units/mL of penicillin G, and 115 μg/mL of streptomycin, in 5% CO_2 cell incubator at 37 °C. Then 100 μL cell suspensions (1000 to 5000 cells) were added into each well of 96-well plates depending on growth rate and allowed to adhere in the incubator. After that, tested samples at pre-set concentrations were added to 96 wells with colchicine as positive reference. After 48h incubation, 10 μL of PBS containing 5 mg/mL of MTT was added to each well. The plates were incubated for further 4 h and then were centrifuged at 1500 rpm for 10 min to remove supernatant. After 150 mL of DMSO was added to each well, the plates were shaken vigorously for 10 min to ensure complete solubilization. The absorbance was measured and recorded on an ELISA reader (ELx800, BioTek, USA) at a test wavelength of 490 nm. In all the experiments three replicate wells were used for each drug concentration. Each assay was carried out at least three times.

4.3.2. Tubulin polymerization assay

Tubulin was purified from bovine brain as described previously. [25, 26] To characterize the effect of the compounds on tubulin assembly *in vitro*, different concentrations of compounds were incubated with 10 μM bovine brain tubulin in glutamate buffer at 30 °C and then cooled to 0 °C. After 0.4 mM GTP added, the mixtures were transferred to cuvettes at 0 °C in a recording spectrophotometer and warmed up to 30 °C. Finally, the assembly of tubulin was observed turbidimetrically at 350 nm. The IC_{50} was defined as the compound concentration inhibited the extent of assembly by 50% after 20 min incubation.

4.3.3. Cell Cycle Analysis

View Article Online
DOI: 10.1039/C5RA28141E

A549 cells were plated in a 6-well plate (5.0×10^5 cells/well) and incubated at 37 °C for 24 h. Then the cells were treated with **6q** at 0, 0.02, 0.05, 0.1, 0.15 and 0.2 μM for 24 h. Treated cells were washed with PBS and fixed with 70% ice-cold ethanol overnight. Then, fixed cells were resuspended in PBS containing 0.1 mg/mL RNase A and 5 μg/mL propidium iodide (PI) and stained at 37 °C for 30 min. Cell cycle distribution was analyzed by BD Accuri C6 Flow Cytometer (BD, USA). The percentage of cells in the G1, S and G2/M phases of the cell cycle were determined using the Flowjo 7.6.1 software after cell debris exclusion.

4.3.4. Annexin-V Assay

A549 cells were plated into a 12-well plate (2.0×10^5 cells/well) and were allowed to adhere for 12 h. After that, the cells were treated with **6q** at final concentrations of 0, 0.05, 0.1 and 0.15 μM for 24 h. Then cells were collected and washed twice with precooled PBS and strained with 10 μL of Annexin V-FITC and 5 μL of PI (5 μg/mL) in 1 × binding buffer for 30 min in the dark. Apoptotic cells were monitored on BD Accuri C6 Flow Cytometer (BD, USA). Statistics were analyzed by Flowjo 7.6.1 software.

4.3.5. Confocal microscopy assay

A549 cells were seeded on glass coverslips and incubated with 0.5 μM paclitaxel, 0.5 μM colchicine and 0.2 μM **6q**, for 24 h respectively. Cells were then rinsed with PBS for three times, fixed with 4% paraformaldehyde for 20 min and permeabilized with cold formaldehyde for 10 min. After that, fixed cells were washed with PBS and blocked with 5% Albumin from bovine serum (BSA) for at least 1 h. After washed with PBS once, the cells were incubated with anti-tubulin antibody (1:500) in 3% BSA overnight at 4 °C, followed by Cy3-labeled goat anti-mouse IgG (H + L) (1: 500) in 3% BSA and incubated for 1 h. Subsequently, the cells were incubated with DAPI (5 ng/mL). Images were captured with Olympus confocal microscope and data was analyzed using FV-10-ASW.

View Article Online
DOI: 10.1039/C5RA28141E

4.4. Docking simulations

Molecular docking of compound **6q** into the three dimensional X-ray structure of tubulin (PDB code: 1SA0) was carried out using the DS 3.5 (Discovery Studio 3.5) as implemented through the graphical user interface DS-CDOCKER protocol. All bound water and ligands were eliminated from the protein and the polar hydrogen was added. The whole tubulin complex was defined as a receptor and the site sphere was selected based on the ligand binding location of colchicine (CN2700), then the CN2700 molecule was removed and replaced by **6q** during the molecular docking procedure. Types of interactions of the docked protein with ligand were analyzed after the end of molecular docking.

4.5. 3D-QSAR

Ligand-based 3D-QSAR approach was performed by QSAR software of DS 3.5. The training sets consisted of inhibitors with the corresponding pIC_{50} values which were converted from the obtained IC_{50} (μM), and test sets comprised compounds of data sets. All the definition of the descriptors could be seen in the "Help" of DS 3.5 software and they were calculated by QSAR protocol of DS 3.5. The alignment conformation of each molecule was the one with lowest interaction energy in the docked results of CDOCKER. The predictive ability of 3D-QSAR modeling can be evaluated based on the cross-validated correlation coefficient, which qualifies the predictive ability of the models. Scrambled test (Y scrambling) was performed to investigate the risk of chance correlations. The inhibitory potencies of compounds were randomly reordered for 30 times and subject to leave-one-out validation test respectively. The models were also validated by test sets, in which the compounds were not included in the training sets.

Acknowledgements

The work was financed by the Projects (Nos. CXY1409 & CG1305) from the

View Article Online
DOI: 10.1039/C5RA28141E

Science & Technology Bureau of Lianyungang City of Jiangsu Province.

References

1. K. N. Bhalla, *Oncogene*, 2003, **22**, 9075-9086.
2. M. A. Jordan and L. Wilson, *Nat. Rev. Cancer*, 2004, **4**.
3. B. A. Teicher, *Clinical Cancer Research*, 2008, **14**, 1610-1617.
4. K. H. Downing and E. Nogales, *Curr. Opin. Struc. Biol*, 1998, **8**, 785-791.
5. S. Honore, E. Pasquier and D. Braguer, *Cellular & Molecular Life Sciences Cmls*, 2006, **62**, 3039-3056.
6. N. G. Kyoko, W. Pei-Chi, L. Chin-Yu, H. Ernest, Z. Hao, Z. Liying, K. Takashi, O. Emika, G. Masuo and K. F. Bastow, *J. Med. Chem*, 2011, **54**, 1244-1255.
7. R. B. G. Ravelli, B. Gigant, P. A. Curmi, I. Jourdain, S. Lachkar, A. Sobel and M. Knossow, *Nature*, 2004, **428**, 198-202.
8. J. Zhou and P. Giannakakou, *Curr Med Chem Anticancer Agents*, 2005, **volume 5**, 65-71.
9. K. Gaukroger, J. A. Hadfield, L. A. Hepworth, N. J. Lawrence and A. T. Mcgown, *J. Org. Chem*, 2001, **66**, 8135-8138.
10. R. Romeo, B. Pier Giovanni, C. L. Olga, L. C. Carlota, C. Maria Dora, B. Andrea, H. Ernest, C. Longchuan, B. Roberta and B. Giuseppe, *J. Med. Chem*, 2010, **53**, 4248-4258.
11. L. R. Giuseppe, S. Taradas, B. Ruoli, M. C. Edler, S. Roberto, C. Antonio, P. Francesco, M. Lara, G. Valerio and M. Carmela, *J. Med. Chem*, 2009, **52**, 7512-7527.
12. B. L. Flynn, G. S. Gill, D. W. Grobelny, J. H. Chaplin, P. Dharam, A. F. Leske, T. C. Lavranos, D. K. Chalmers, S. A. Charman and K. Edmund, *J. Med. Chem*, 2011, **54**, 6014-6027.
13. Á. Raquel, P. Pilar, D. J Fernando, A. C. Bento, G. N. Rósula, I. V. Janis, M. Faustino, A. José Manuel, M. Manuel and P. Rafael, *J. Med. Chem*, 2013, **56**, 2813-2827.

View Article Online
DOI: 10.1039/C5RA28141E

14. A. Brancale and R. Silvestri, *Med. Res. Rev*, 2007, **27**, 209-238.
15. G. L. Regina, R. Bai, A. Coluccia, V. Famiglini, S. Pelliccia, S. Passacantilli, C. Mazzoccoli, V. Ruggieri, A. Verrico and A. Miele, *J. Med. Chem*, 2015.
16. E. J. Solum, J. J. Cheng, I. B. Sørvik, R. E. Paulsen, A. Vik and T. V. Hansen, *Eur. J. Med. Chem*, 2014, **85**, 391-398.
17. R. Romagnoli, P. G. Baraldi, T. Sarkar, M. D. Carrion, C. L. Cara, O. Cruz-Lopez, D. Preti, M. A. Tabrizi, M. Tolomeo and S. Grimaudo, *J. Med. Chem*, 2008, **51**, 1464-1468.
18. A. Tanitame, Y. Oyamada, K. Ofuji, M. Fujimoto, N. Iwai, Y. Hiyama, K. Suzuki, H. Ito, H. Terauchi and M. Kawasaki, *J. Med. Chem*, 2004, **47**.
19. T. D. Penning, J. J. Talley, S. R. Bertenshaw, J. S. Carter, P. W. Collins, S. Docter, M. J. Graneto, L. F. Lee, J. W. Malecha and J. M. Miyashiro, *J. Med. Chem*, 1997, **40**, 1347-1365.
20. M. Johnson, B. Younglove, L. Lee, R. Leblanc, H. Holt, P. Hills, H. Mackay, T. Brown, S. L. Mooberry and M. Lee, *Bioorg. Med. Chem. Lett*, 2007, **17**, 5897-5901.
21. S. K. Tahir, E. K. Han, B. Credo, H. S. Jae, J. A. Pietenpol, C. D. Scatena, J. R. Wu-Wong, D. Frost, H. Sham and S. H. Rosenberg, *Cancer. Res*, 2001, **61**, 5480-5485.
22. Y. Hu, X. Lu, K. Chen, R. Yan, Q. S. Li and H. L. Zhu, *Bioorgan. Med. Chem*, 2012, **20**, 903-909.
23. Y. T. Wang, Y. J. Qin, N. Yang, Y. L. Zhang, C. H. Liu and H. L. Zhu, *Eur. J. Med. Chem*, 2015, **99**, 125-137.
24. J. M. Cole, *Acta Crystallographica*, 2008, **64**.
25. E. Hamel and C. M. Lin, *Biochemistry-US*, 1984, **23**, 4173-4184.
26. A. M. Minotti, S. B. Barlow and F. Cabral, *J. Biol. Chem*, 1991, **266**, 3987-3994.

View Article Online
DOI: 10.1039/C5RA28141E

Figure captions:

Table 1. Structures of compounds **6a-6v**

Table 2. Crystallographic and experimental data for compound **6o**

Table 3. *In vitro* inhibitory effects of compounds **6a-6v** against human tumor cell lines, normal cell line and tubulin polymerization

Table 4. The experimental and predicted inhibitory activity of compounds (**6a-6v**) by 3D-QSAR models based upon active conformation achieved by molecular docking

Figure 1. Chemical structures of inhibitors and potential inhibitors of tubulin polymerization

Figure 2. Crystal structure diagram of compound **6o**. H atoms are shown as small spheres of arbitrary radii.

Figure 3. Correlation between the anti-proliferative activity against A549 cell line and the tubulin polymerization inhibitory activity of the top 10 compounds

Figure 4. Effect of compound **6q** on cell cycle progression of A549 cells was determined by flow cytometry analysis. (G1 phase, blue; S phase, yellow and G2/M phase, green)

Figure 5. Representative Scatter Plot of A549 cells treated with **6q** at 0, 0.05, 0.1 and 0.15 μM and analyzed by flow cytometry after double staining of the cells with Annexin-V-FITC and PI.

Figure 6. Effects of paclitaxel (0.5 μM), colchicine (0.5 μM) and **6q** (0.2 μM) on cellular architecture and microtubule network of A549 cells. Microtubules tagged with Cy3 (red) and nuclei tagged with DAPI (blue) were observed with a confocal microscope.

Figure 7. The binding mode between the active conformation of compound **6q** and the target protein tubulin (PDB code: 1SA0) provided by the CDOCKER protocol (Discovery Studio 3.5, Accelrys, Co. Ltd). **(A)**. The receptor surface model with compound **6q**; **(B)**. 3D diagram of the interactions between colchicine (burlywood) & **6q** (cyan) and the colchicine binding site. Only interacting residues are displayed. The H-bond (green arrow) is displayed as dotted arrows; **(C)**. 2D diagram of the

View Article Online
DOI: 10.1039/C5RA28141E

interactions between colchicine and the colchicine binding site; **(D)**. 2D diagram of the interactions between compound **6q** and the colchicine binding site. The H-bond (green arrow) is displayed as dotted arrows.

Figure 8. Comparing the predicted pIC_{50} value of tubulin inhibitory activities with that of the experiment by linear fitting curve

Figure 9. (A). Isosurface of the 3D-QSAR model coefficients on electrostatic potential grids. Blue represents positive coefficients; red represents negative coefficients. **(B).** Isosurface of the 3D-QSAR model coefficients on Van der Waals grids. Green represents positive coefficients; yellow represents negative coefficients.

Scheme 1. General synthesis of compounds **6a-6v**

View Article Online
DOI: 10.1039/C5RA28141E

Table 1. Structures of compounds **6a-6v**

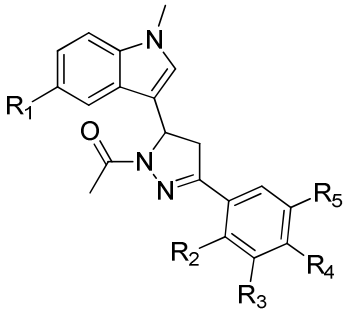

Compounds	R_1	R_2	R_3	R_4	R_5
6a	H	H	H	H	H
6b	H	H	H	OCH_3	H
6c	H	H	OCH_3	OCH_3	H
6d	H	H	OCH_3	OCH_3	OCH_3
6e	H	H	H	Cl	H
6f	H	H	H	Br	H
6g	H	H	H	CF_3	H
6h	OCH_3	H	H	H	H
6i	OCH_3	H	H	OCH_3	H
6j	OCH_3	H	OCH_3	OCH_3	H
6k	OCH_3	H	H	F	H
6l	OCH_3	H	H	Cl	H
6m	OCH_3	H	H	Br	H
6n	Br	H	H	H	H
6o	Br	OCH_3	H	H	H
6p	Br	H	OCH_3	H	H
6q	Br	H	H	OCH_3	H
6r	Br	H	OCH_3	OCH_3	H
6s	Br	H	OCH_3	OCH_3	OCH_3
6t	Br	H	H	F	H
6u	Br	H	H	Cl	H
6v	Br	H	H	Br	H

View Article Online
DOI: 10.1039/C5RA28141E

Table 2. Crystallographic and experimental data for compound **6o**

Compound	**6o**
Formula	$C_{21}H_{20}BrN_3O_2$
Formula weight	426.31
Crystal system	Monoclinic
Space group	*P 21/c*
a (Å)	16.5763(14)
b (Å)	8.0259(7)
c (Å)	15.6946(13)
α (°)	90
β (°)	109.896(2)
γ (°)	90
V (Å^3)	1963.4(3)
Z	4
D_c (g cm^{-3})	1.442
F (000)	872
θ rang (°)	2.62-25.06
Reflections collected/unique	16844/3457
Data/restraints/parameters	3457/0/247
Absorption coefficient (mm^{-1})	2.114
Goodness-of-fit on F^2	1.050
R_1, wR_2 [$I > 2\sigma(I)$]	0.0494, 0.1100
R_1, wR_2 [all data]	0.0821, 0.1265
Max, min $\Delta\rho$ (e Å^{-3})	0.578, -0.653

View Article Online
DOI: 10.1039/C5RA28141E

Table 3. *In vitro* inhibitory effects of compounds **6a-6v** against human tumor cell lines, normal cell line and tubulin polymerization

Compounds	IC_{50}±SD (μM)				
	A549[a]	MCF-7[a]	HepG2[a]	293T[b]	Tubulin[c]
6a	5.18 ± 1.03	6.35 ± 0.33	9.22 ± 1.98	105.41 ± 4.04	32.53 ± 1.97
6b	0.19 ± 0.02	0.22 ± 0.01	0.26 ± 0.08	129.37 ± 3.93	4.33 ± 0.24
6c	4.52 ± 0.12	5.27 ± 0.68	5.46 ± 0.29	234.10 ± 4.50	23.19 ± 1.46
6d	2.36 ± 0.23	3.03 ± 0.23	3.12 ± 0.20	269.48 ± 3.84	11.45 ± 0.53
6e	1.68 ± 0.39	1.43 ± 0.05	2.24 ± 0.08	48.68 ± 6.05	22.02 ± 1.19
6f	0.87 ± 0.11	1.46 ± 0.36	1.71 ± 0.11	>300	14.32 ± 0.41
6g	1.24 ± 0.18	2.40 ± 0.31	1.92 ± 0.56	139.34 ± 0.82	26.14 ± 0.47
6h	11.75 ± 1.29	13.21 ± 0.13	14.09 ± 0.15	298.46 ± 3.19	34.96 ± 1.34
6i	0.22 ± 0.02	0.31 ± 0.11	0.34 ± 0.09	243.59 ± 6.11	5.75 ± 0.17
6j	8.31 ± 0.41	10.09 ± 0.52	9.76 ± 1.78	187.09 ± 1.41	19.62 ± 0.55
6k	4.92 ± 0.73	5.78 ± 0.07	6.63 ± 0.17	168.46 ± 5.85	13.05 ± 0.20
6l	6.43 ± 0.14	8.12 ± 0.36	7.93 ± 0.16	>300	19.76 ± 1.95
6m	1.42 ± 0.29	1.60 ± 0.27	1.88 ± 0.24	134.51 ± 1.89	10.39 ± 0.18
6n	1.08 ± 0.27	1.51 ± 0.47	1.20 ± 0 03	32.79 ± 0.68	20.54 ± 0.40
6o	0.71 ± 0.34	0.85 ± 0.13	0.92 ± 0.13	>300	15.92 ± 0.81
6p	1.24 ± 0.26	0.97 ± 0.25	1.14 ± 0.21	205.86 ± 2.67	29.64 ± 2.68
6q	0.15 ± 0.03	0.17 ± 0.05	0.25 ± 0.05	245.92 ± 3.44	1.98 ± 0.25
6r	0.51 ± 0.01	0.55 ± 0.02	0.54 ± 0.09	89.18 ± 2.52	10.03 ± 0.50
6s	0.31 ± 0.04	0.38 ± 0.09	0.42 ± 0.06	>300	7.81 ± 0.39
6t	0.21 ±0.10	0.19 ± 0.04	0.29 ± 0.01	100.23 ± 4.67	4.22 ± 0.13
6u	0.24 ±0.07	0.27 ± 0.12	0.34 ± 0.04	79.68 ± 2.88	5.85 ± 0.37
6v	0.18 ± 0.01	0.20 ± 0.04	0.26 ± 0.05	46.46 ± 1.34	3.16 ± 0.42
Colchicine[d]	0.21 ± 0.06	0.22 ± 0.12	0.32 ± 0.09	172 ± 5.52	2.35 ± 0.34

All experiments were independently performed at least three times.

[a] Inhibition of the growth of tumor cell lines

[b] Inhibition of the growth of nomal cell line

[c] Inhibition of tubulin polymerization

[d] Used as positive control

View Article Online
DOI: 10.1039/C5RA28141E

Table 4. The experimental and predicted inhibitory activity of compounds (**6a-6v**) by 3D-QSAR models based upon active conformation achieved by molecular docking

Compounds	Tubulin Assembly		Residual error
	Actual pIC_{50}	Predicted pIC_{50}	
6a	4.488	4.480	0.008
6b	5.364	5.380	-0.016
6c	4.635	4.640	-0.005
6d	4.941	4.930	0.011
6e	4.657	4.793	-0.136
6f	4.844	4.885	-0.041
6g	4.583	4.556	0.027
6h	4.456	4.797	-0.341
6i	5.240	5.219	0.021
6j	4.707	4.713	-0.006
6k	4.884	4.857	0.027
6l	4.704	4.719	-0.015
6m	4.983	4.989	-0.006
6n	4.687	4.718	-0.031
6o	4.772	4.682	0.090
6p	4.528	4.525	0.003
6q	5.703	5.688	0.015
6r	4.999	4.988	0.011
6s	5.107	5.098	0.009
6t	5.375	5.385	-0.010
6u	5.233	5.238	-0.005
6v	5.500	5.504	-0.004

[a] The underlined for the test set, and the rest for training

View Article Online
DOI: 10.1039/C5RA28141E

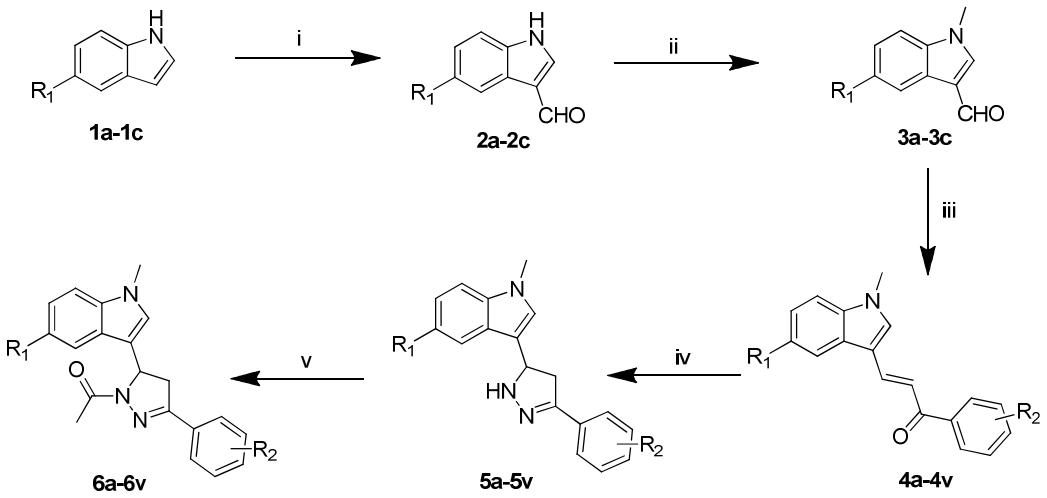

Scheme 1. General synthesis of compounds **6a-6v**. Reagents and conditions: (i) DMF, $POCl_3$, 0 °C, 2 h; (ii) CH_3I, NaH, THF, 0 °C - r.t., 24 h; (iii) Substituted acetophenone, KOH, EtOH, r.t., 24 h; (iv) $N_2H_4 \cdot H_2O$, EtOH, reflux, 2h; (v) AcOH, EDC·HCl, HOBt, CH_3CN/CH_2Cl_2, r.t., 24 h.

View Article Online
DOI: 10.1039/C5RA28141E

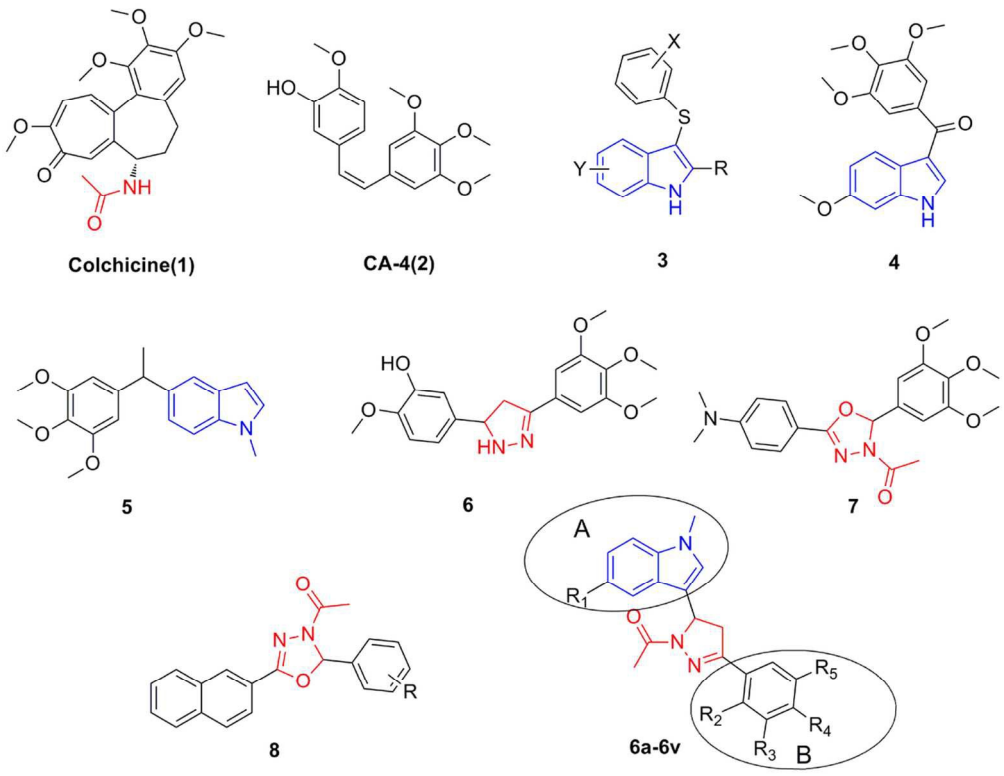

Figure 1. Chemical structures of inhibitors and potential inhibitors of tubulin polymerization
108x83mm (300 x 300 DPI)

View Article Online
DOI: 10.1039/C5RA28141E

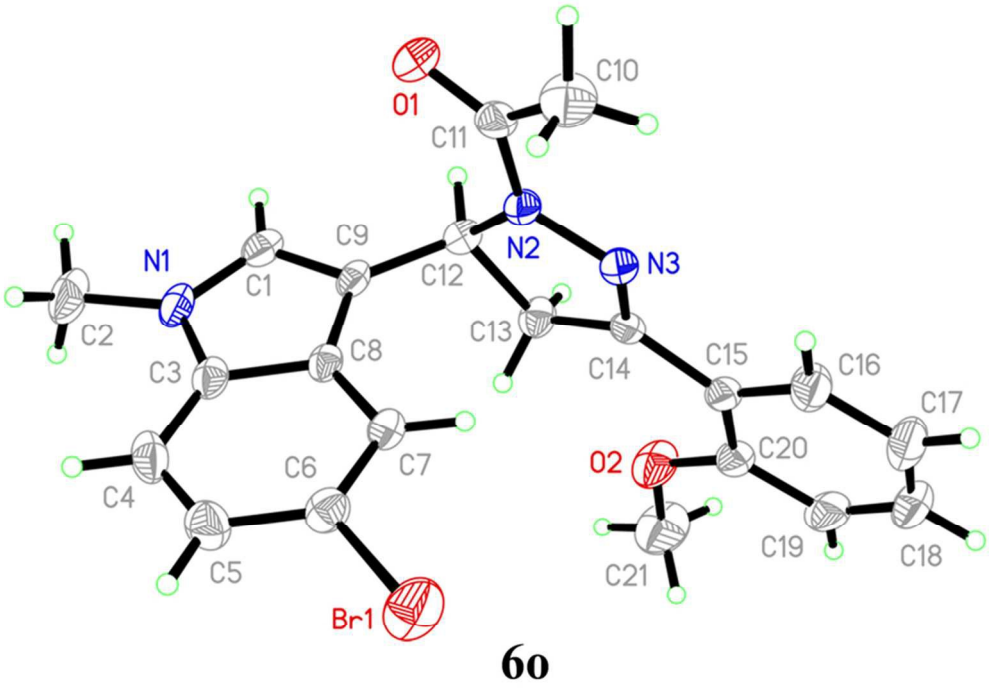

6o

Figure 2. Crystal structure diagram of compound 6o. H atoms are shown as small spheres of arbitrary radii.
79x63mm (300 x 300 DPI)

View Article Online
DOI: 10.1039/C5RA28141E

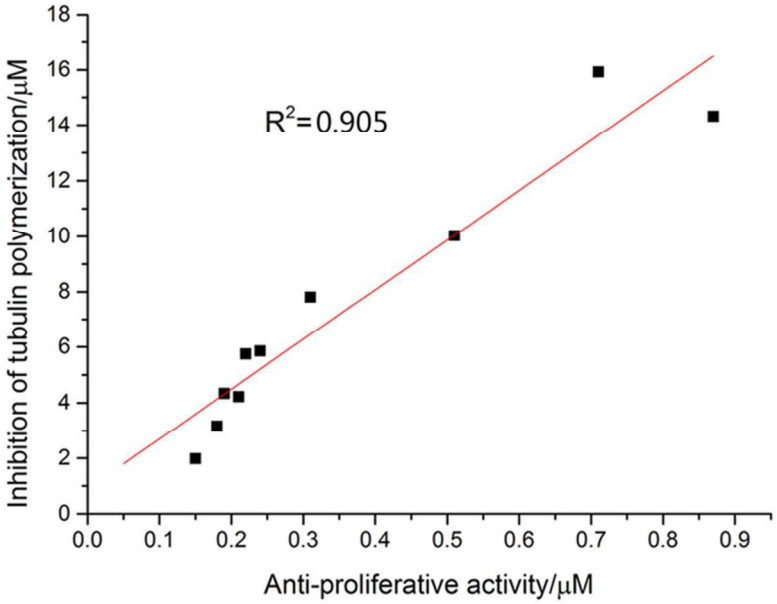

Figure 3. Correlation between the anti-proliferative activity against A549 cell line and the tubulin polymerization inhibitory activity of the top 10 compounds
69x48mm (300 x 300 DPI)

View Article Online
DOI: 10.1039/C5RA28141E

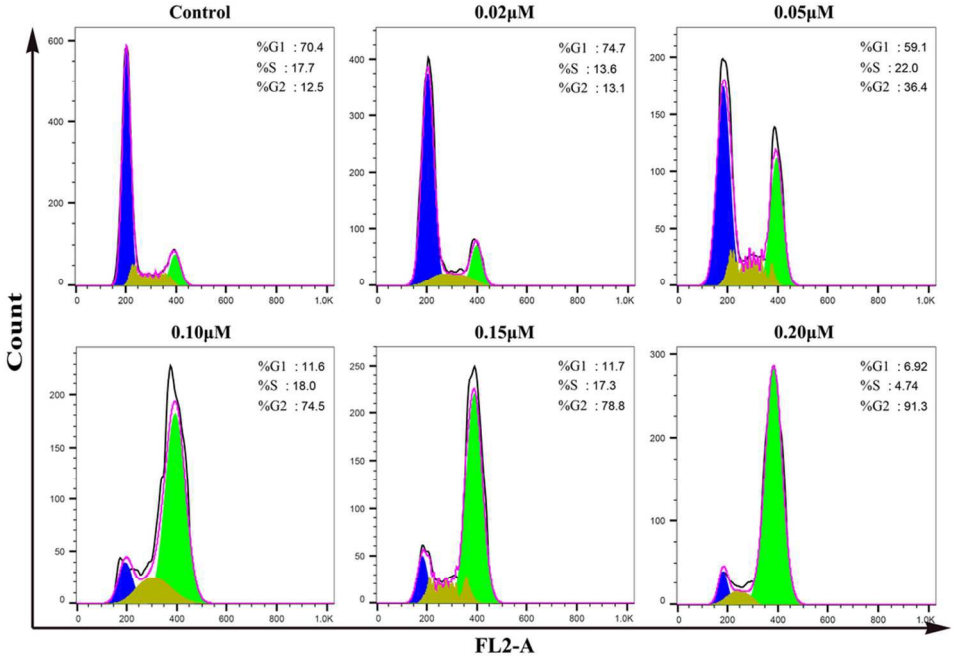

Figure 4. Effect of compound 6q on cell cycle progression of A549 cells was determined by flow cytometry analysis. (G1 phase, blue; S phase, yellow and G2/M phase, green)
97x67mm (300 x 300 DPI)

View Article Online
DOI: 10.1039/C5RA28141E

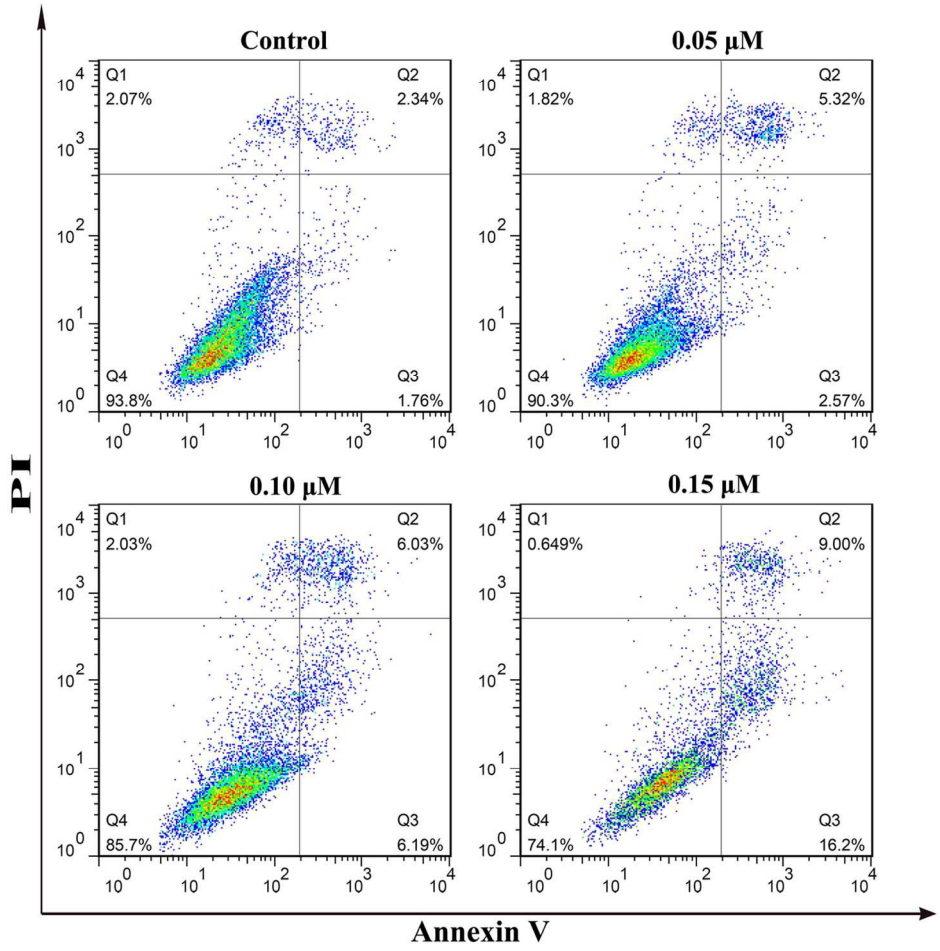

Figure 5. Representative Scatter Plot of A549 cells treated with 6q at 0, 0.05, 0.1 and 0.15 µM and analyzed by flow cytometry after double staining of the cells with Annexin-V-FITC and PI.
136x133mm (300 x 300 DPI)

View Article Online
DOI: 10.1039/C5RA28141E

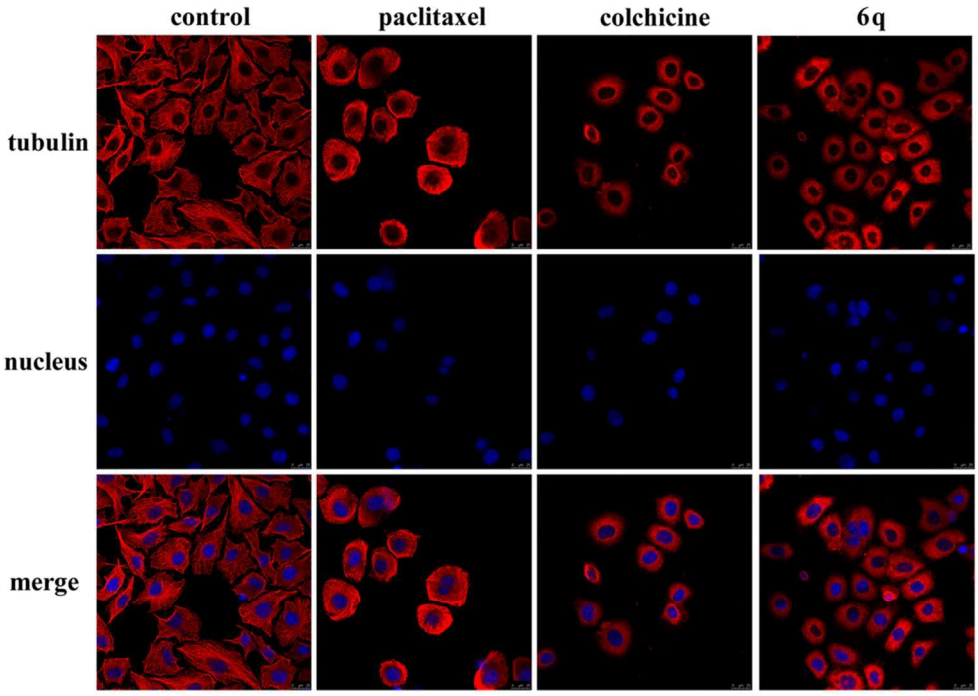

Figure 6. Effects of paclitaxel (0.5 μM), colchicine (0.5 μM) and 6q (0.2 μM) on cellular architecture and microtubule network of A549 cells. Microtubules tagged with Cy3 (red) and nuclei tagged with DAPI (blue) were observed with a confocal microscope.
100x71mm (300 x 300 DPI)

View Article Online
DOI: 10.1039/C5RA28141E

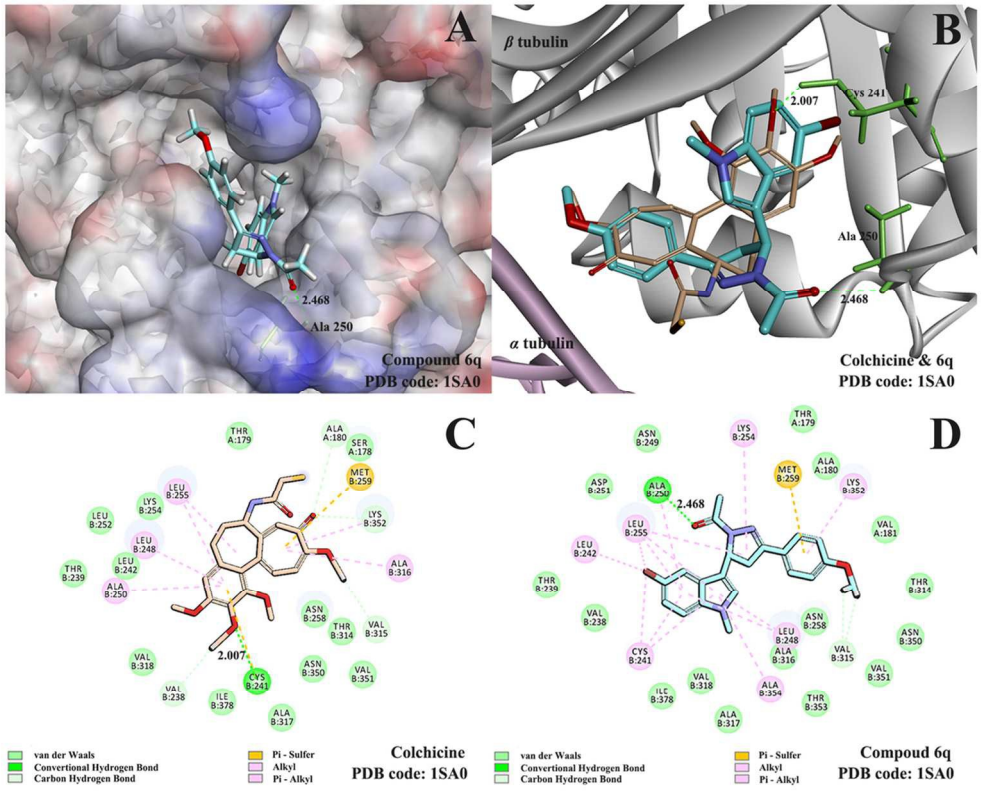

Figure 7. The binding mode between the active conformation of compound 6q and the target protein tubulin (PDB code: 1SA0) provided by the CDOCKER protocol (Discovery Studio 3.5, Accelrys, Co. Ltd). (A). The receptor surface model with compound 6q; (B). 3D diagram of the interactions between colchicine (burlywood) & 6q (cyan) and the colchicine binding site. Only interacting residues are displayed. The H-bond (green arrow) is displayed as dotted arrows; (C). 2D diagram of the interactions between colchicine and the colchicine binding site; (D). 2D diagram of the interactions between compound 6q and the colchicine binding site. The H-bond (green arrow) is displayed as dotted arrows.
112x89mm (300 x 300 DPI)

View Article Online
DOI: 10.1039/C5RA28141E

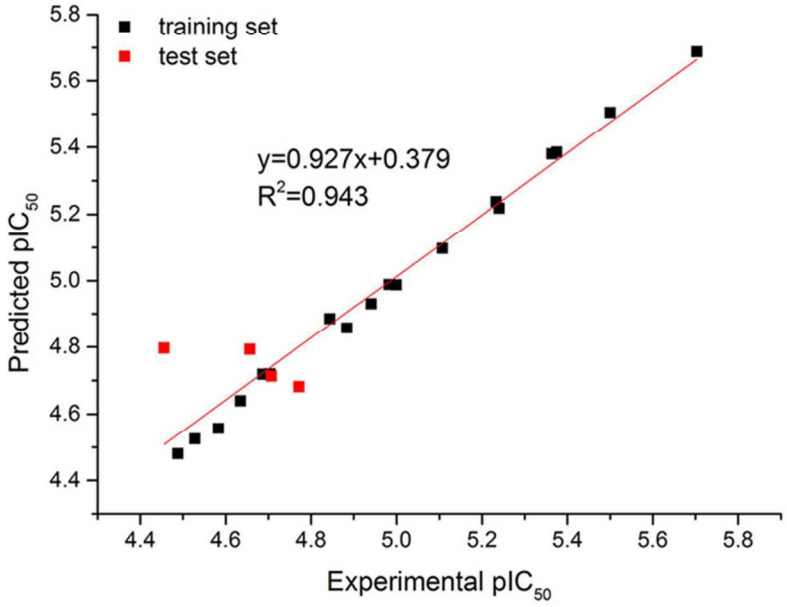

Figure 8. Comparing the predicted pIC50 value of tubulin inhibitory activities with that of the experiment by linear fitting curve
69x48mm (300 x 300 DPI)

View Article Online
DOI: 10.1039/C5RA28141E

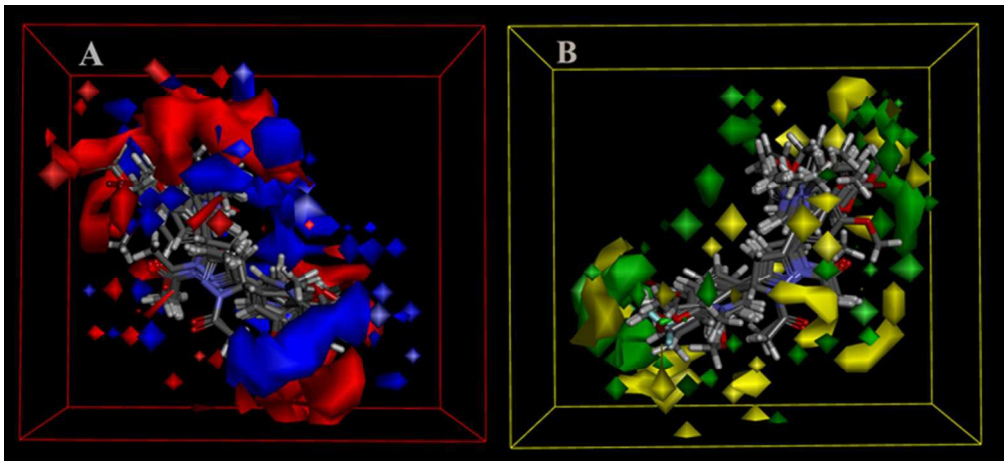

Figure 9. (A). Isosurface of the 3D-QSAR model coefficients on electrostatic potential grids. Blue represents positive coefficients; red represents negative coefficients. (B). Isosurface of the 3D-QSAR model coefficients on Van der Waals grids. Green represents positive coefficients; yellow represents negative coefficients.
63x28mm (300 x 300 DPI)

View Article Online
DOI: 10.1039/C5RA28141E

Synthesis, biological evaluation and molecular docking studies of novel 1-(4,5-dihydro-1*H*-pyrazol-1-yl)ethanone-containing 1-methylindol derivatives as potential tubulin assembling inhibitors

Meng-Ru Yang[†a], Ya-Juan Qin[†a], Chen Chen[a], Ya-Liang Zhang[a], Bo-Yan Li[a], Tian-Bao Liu[a], Hai-Bin Gong*[b], Bao-Zhong Wang*[a], Hai-Liang Zhu*[a]

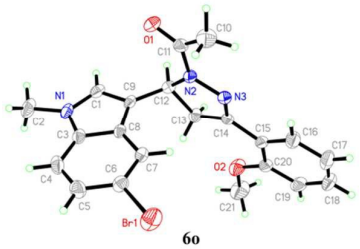

6o

A series of novel compounds (**6a-6v**) containing 1-methylindol and 1-(4,5-dihydro-1*H*-pyrazol-1-yl)ethanone skeleton were designed, synthesized and evaluated as potential anticancer agents.